Molecular Plant
Research Article

CellPress
PARTNER JOURNAL

Folate Metabolism Interferes with Plant Immunity through 1C Methionine Synthase-Directed Genome-wide DNA Methylation Enhancement

Beatriz González and Pablo Vera*

Instituto de Biología Molecular y Celular de Plantas, Universidad Politécnica de Valencia-C.S.I.C, Ciudad Politécnica de la Innovación, Edificio 8E, Ingeniero Fausto Elio, s/n, 46022 Valencia, Spain

*Correspondence: Pablo Vera (vera@ibmcp.upv.es)

https://doi.org/10.1016/j.molp.2019.04.013

ABSTRACT

Plants rely on primary metabolism for flexible adaptation to environmental changes. Here, through a combination of chemical genetics and forward genetic studies in *Arabidopsis* plants, we identified that the essential folate metabolic pathway exerts a salicylic acid-independent negative control on plant immunity. Disruption of the folate pathway promotes enhanced resistance to *Pseudomonas syringae* DC3000 via activation of a primed immune state in plants, whereas its implementation results in enhanced susceptibility. Comparative proteomics analysis using immune-defective mutants identified a methionine synthase (METS1), in charge of the synthesis of Met through the folate-dependent 1C metabolism, acting as a nexus between the folate pathway and plant immunity. Overexpression of *METS1* represses plant immunity and is accompanied by genome-wide global increase in DNA methylation, revealing that imposing a methylation pressure at the genomic level compromises plant immunity. Take together, these results indicate that the folate pathway represents a new layer of complexity in the regulation of plant defense responses.

Key words: folate pathway, plant immunity, methionine, DNA methylation

González B. and Vera P. (2019). Folate Metabolism Interferes with Plant Immunity through 1C Methionine Synthase-Directed Genome-wide DNA Methylation Enhancement. Mol. Plant. **12**, 1227–1242.

INTRODUCTION

To prevent microbial growth, plants rely on efficient resistance mechanisms that involve complex signaling networks orchestrating inducible and durable defenses. These responses include physical changes (e.g., cell wall fortification [Hardham et al., 2007]) and biochemical responses (e.g., production of reactive oxygen species [Torres, 2010] or signaling compounds such as salicylic acid [SA] [Vlot et al., 2009] and other pathogen-related hormones [Pieterse et al., 2012]) that perturb infection (Jones and Dangl, 2006). In the massive reprogramming of the plant cell following recognition of pathogens, the transcriptional activation/repression of a selective set of genes is also a common signature of an immune response. This precedes *de novo* production of various defense-related proteins and secondary metabolites, including phytoalexins and various phenolic compounds that contribute to the resistance response (van Loon et al., 2006; Ahuja et al., 2012). The activation of diverse defense pathways in the host is associated with increase demand for energy and carbon skeletons that are provided by primary metabolic pathways (Bolton, 2009; Kangasjarvi et al., 2012). Consistent with this, decreases in photosynthesis and chlorophyll biosynthesis are characteristic plant responses to pathogen attack (Berger et al., 2004; Denoux et al., 2008; Bilgin et al., 2010; García-Andrade et al., 2013) that likely alleviates the energy expenditure associated with the upregulation of other pathways that contribute to disease resistance. Amino acid metabolism is another example as to how distinct metabolic pathways constitute integral parts of the immune system in plants. For instance, lysine catabolism is required for the synthesis of pipecolic acid, a critical regulator of plant systemic acquired resistance (Navarova et al., 2012), and evidence suggests that accumulation of some amino acids or their metabolic by-products triggers resistance (Zeier, 2013). Thus, reconfiguration of primary metabolism is key in the regulation of immune responses, although still more studies are needed to identify additional components and pathways involved in the control of plant immunity.

Among the mechanisms involved in cell reprogramming during defense, the importance of epigenetic control is emerging as an additional layer of complexity in the control of plant

Published by the Molecular Plant Shanghai Editorial Office in association with Cell Press, an imprint of Elsevier Inc., on behalf of CSPB and IPPE, SIBS, CAS.

immunity (López et al., 2011; Yu et al., 2013). DNA methylation is a conserved epigenetic marker, important for development and stress adaptation in plants, and has been implicated in the transmission of a priming state or stress memory endowing progeny of pathogen-inoculated plants with heightened resistance (transgenerational induced resistance), suggesting that plants can inherit priming sensitization (Luna et al., 2012; Slaughter et al., 2012). Epigenetic mechanisms regulating gene expression programs are similarly under the control of primary metabolic flux, which ultimately controls the activity of enzymes involved in DNA methylation and histone modifications (Shen et al., 2016). In this respect, recent findings indicate that epigenetic regulation of gene expression is under the control of the folate-dependent one-carbon (1C) metabolism, which ultimately produces *S*-adenosylmethionine (SAM), the universal donor utilized by most methyltransferase to methylate DNA and histones. Consistently, pharmacological impairment of the folate pathway suppresses epigenetic gene silencing and release expression of transgenes as well as endogenous transposons, whereas application of compounds of the folate pathway restores transcriptional silencing (Zhang et al., 2012). Moreover, hypomorphic mutants in *HOMOLOGY-DEPENDENT GENE SILENCING* (*HOG1*) (Rocha et al., 2005), *FOLILPOLYGUTAMATE SYNTHASE* (*FPGS1*) (Zhou et al., 2013), and *METHYLENETETRAHYDROFOLATE DESHY DROGENASE* (*MTHFD1*) (Groth et al., 2016), defective in folate-dependent 1C metabolism and, in turn, in SAM accumulation, show reduced DNA methylation and release chromatin silencing on a genome-wide scale. This denotes the interplay between primary metabolism and epigenetic regulation that is essential for plant adaptation. Since plant immunity is under epigenetic control (López et al., 2011; Yu et al., 2013), the metabolic pathways exerting control over epigenetic mechanisms of gene expression may also impart control over immune responses. However, in the continued focus on pathogen recognition and downstream signaling in plant defense activation, the recruitment of components of primary metabolism to modulate plant immunity has received poor attention or has passed unnoticed in genetic screens, presumably due to the existence of genetic redundancy or essentiality of the pathway. Here, we report the identification of a series of sulfonamide derivatives, identified through a chemical genetic screen in the search for agonists of plant immunity, which promote primed immunity in *Arabidopsis*. Sulfonamides disrupt folate metabolism, and we identified that the folate pathway exerts an SA-independent negative control over immune responses toward *Pseudomonas syringae* DC3000 (*P.s.* DC3000). Moreover, we identified that accumulation of a 5-METHYLTETRAHYDROPTEROYLTRIGLUTAMATE HOMOCYSTEINE METHYLTRANSFERASE1 (methionine synthase; METS1), which carries the synthesis of Met through the folate-dependent 1C metabolism required to produce SAM for transmethylation reactions, impairs plant immunity and leads to enhanced disease susceptibility. Genome-wide increase in CG, CHG, and CHH methylation accompanies *METS1* overexpression, implying that an imposed methylation pressure at the genome level interferes with plant immunity. These observations uncover the existence of interplay between plant immunity and epigenetic regulation whereby folate primary metabolism acts as a nexus.

RESULTS

Sulfonamides Promote Transcriptional Activation of *Ep5C*::*GUS*

Previously, the defense-related *Ep5C* gene promoter fused to β-glucuronidase (*Ep5C*::*GUS*) was used as reporter in forward genetic screenings designed to identify repressors of plant immune responses in *Arabidopsis*. As a result, mutants defective in AGO4 (i.e., *ocp11*) (Agorio and Vera, 2007) or NRPD2/RNA PolV (i.e., *ocp1*) (López et al., 2011) were identified that showed constitutive expression of *Ep5C*::*GUS* accompanied by altered immunity. These findings revealed the importance of epigenetic control in the regulation of plant immunity. Now, in search for agonist molecules of plant immunity, we performed a forward chemical genetic screen using the *Arabidopsis Ep5C*::*GUS* marker line. The Library of Active Compounds in *Arabidopsis* (LATCA) (http://cutlerlab.blogspot.com/2008/05/latca.html) was used as a source of biologically active small molecules. We screened the chemicals in this library at 25 μM in triplicate. In the screening, potential chemical activators of *Ep5C*::*GUS* were evaluated based on visualization of GUS activity upon histochemical staining of treated seedlings. From the 3650 compounds analyzed, we identified eight hits that promoted strong transcriptional activation of *Ep5C*::*GUS* (Figure 1A). The eight compounds represented chemical variants of sulfonamides (i.e., sulfabenzamide [SB], sulfamethazine [SMZ], sulfaguanidine [SGN], dapsone [DAP], sulfathiazole [STH], sulfachlorpyridazine [SCH], sulfadiazine [SDZ], and sulfamethizole [SMTH]). The compound sulfanilamide (SNL), identified in a structure–activity relationship study (Toth and van der Hoorn, 2010), represents the common moiety of these eight sulfonamides identified in our screening. However, SNL per se promoted weak activation of GUS expression, which occurred only in the seedling roots (Figure 1A). This suggests that the sulfonamide R group appears mandatory for gene activation in these assays. Sulfonamide-mediated gene expression appeared specific for *Ep5C*, since similar analysis performed on a transgenic line carrying a different defense-related reporter gene (i.e., *P69C*::*GUS*), previously shown to be induced by *P.s*. DC3000 and SA (Jordá et al., 1999), showed no effect in promoting transcriptional activation of *P69C*::*GUS* (Figure 1A). This suggests that sulfonamides impinge upon a specific branch of the immune system and only activate a subset of the defense arsenal.

Sulfonamides Promote Deposition of Phosphorylated MPK3 and MPK6 and Poise SA-Related PR1 Protein for Enhanced Accumulation

Constitutive expression of *Ep5C*::*GUS*, as previously observed in *ocp1* and *ocp11* mutants, was associated with a constitutive immune priming phenotype where SA-related genes are poised for enhanced activation (López et al., 2011). Since pre-stress deposition of the phosphorylated mitogen-activated protein kinases (MPKs) MPK3 and MPK6 has been described as the molecular marker for the diagnosis of a priming state in *Arabidopsis* (Beckers et al., 2009), we reasoned that the sulfonamide derivatives identified above could promote activation of MPK3 and MPK6. To address this possibility, we performed Western blot analysis of protein extracts derived from *Arabidopsis* seedlings treated with the different

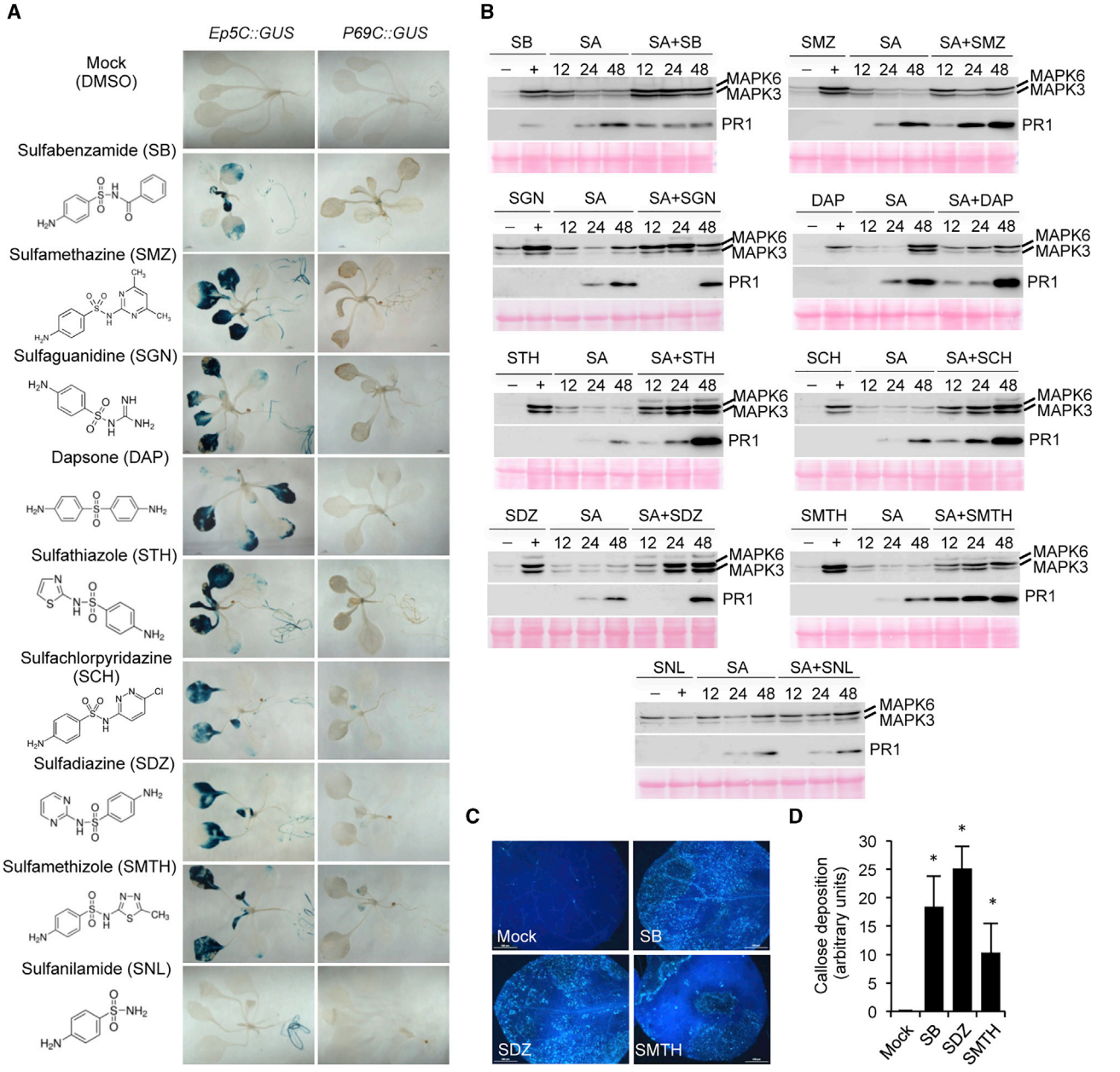

Figure 1. Identification of Sulfonamides Promoting Transcriptional Activation of *Ep5C*::*GUS* and Immune Priming.

(A) Comparative histochemical analysis of GUS activity in *Arabidopsis* seedlings bearing either *Ep5C*::*GUS* or *P69C*::*GUS* gene constructs following incubation with DMSO (mock) or with the different sulfonamide derivatives (25 μM) identified in a chemical genetic screen. A representative 14-day-old seedling of each transgenic line is shown. Scale bars represent 1 mm.

(B) Western blots of protein extracts from control seedlings (–) and seedlings treated with the indicated sulfonamides (+) (two first lines on the left), and from seedlings treated for 12, 24, and 48 h with SA (50 μM) alone or SA (50 μM) plus each of the identified sulfonamides. The blots were incubated with antibodies against MPKs (pTEpY motif) and PR1. Equal protein loading was verified by staining of the nitrocellulose filters with Ponceau-S.

(C and D) Callose deposition in leaves of seedlings treated with the indicated sulfonamides. **(C)** Aniline blue staining and UV fluorescence microscopy was used to visualize callose deposition. Scale bars represent 500 μm. **(D)** Callose deposition was calculated as arbitrary units by quantifying the ratio between the number of yellow pixels (corresponding to callose) and the total number of pixels covering plant material in the digital micrograph (on percentage). Bars represent mean ± SD, $n = 15$ independent replicates. Asterisks indicate statistically significant differences related to non-treated control seedlings (ANOVA simple test; $^*P < 0.05$). These experiments were repeated three times with similar results. Control samples (mock) were incubated with DMSO.

sulfonamide derivatives to identify phosphorylated MPK3 and MPK6 deposition by employing a specific antibody (Jordá et al., 1999; Ramírez et al., 2013). Western blots shown in Figure 1B (first two lanes on the left of each blot) revealed marked activation of MPK3 and MPK6 following treatment with the identified sulfonamides. SNL, which promoted no *Ep5C*::*GUS* activation (Figure 1A), neither promoted enhanced deposition of the two kinases (Figure 1B). These results thus confirm that sulfonamides promote deposition of MAP kinases and anticipate that treated seedlings are in a primed immune state.

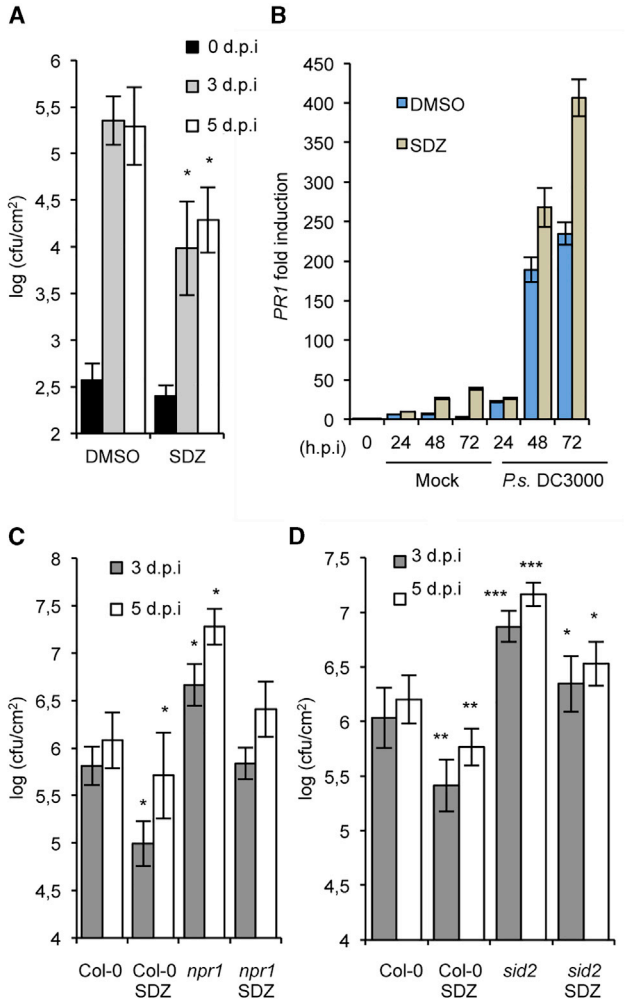

Figure 2. Sulfadiazine Promotes Enhanced Disease Resistance to *P.s.* DC3000.

(A) Growth rate of *P.s.* DC3000 in mock (DMSO)- and sulfadiazine (SDZ) (100 μM)-treated Col-0 plants. Error bars indicate SD of logarithm of colony-forming units (cfu) (n = 12 plants).

(B) qRT–PCR analysis of *PR1* gene expression in mock (DMSO)- and SDZ (100 μM)-treated Col-0 plants following *P.s.* DC3000 inoculation. Samples were taken at 0, 24, 48, and 72 h post inoculation (hpi). Data represent mean ± SD; n = 3 replicates.

(C) Comparison of *P.s.* DC3000 growth rate in mock- and SDZ-treated Col-0 and *npr1* plants.

(D) Comparison of *P.s.* DC3000 growth rate in mock- and SDZ-treated Col-0 and *sid2* plants.

Error bars indicate SD (n = 12 plants). Asterisks indicate statistically significant differences related to Col-0 plants incubated with DMSO. The number of asterisks denote difference levels between data (ANOVA simple test; *P < 0.05).See also Supplemental Figures 1 and 2.

As expected for this immune state, accumulation of SA-related defenses (e.g., PR1 protein accumulation) did not occur by the sole application of the different sulfonamides (Figure 1B, first two lanes on the left of each blot). However, if sulfonamides are promoting a priming immune state in the treated plant, one could expect that SA-related defenses will be poised for more rapid and/or enhanced activation upon application of the defense inducer. Western blots of proteins from seedlings that were treated for 12, 24, and 48 h with 50 μM SA in the absence or presence of each of the nine sulfonamide derivatives identified in the previous screen were immunodecorated with an antibody recognizing the PR1 protein (Ramírez et al., 2013). Most of the sulfonamide analogs sensitized seedlings for an SA-induced accumulation of PR1, which occurred either faster, already visible at 12 h of SA application (i.e., SB, SMZ, DAP, STH, SCH, SMTH), or at higher levels (i.e., SMZ, DAP, SCH, SDZ, SMTH). In the case of SGN, despite showing enhanced deposition of phosphorylated MPK3 and MPK6, we could not detect primed induction of PR1 by SA. As expected, SNL also did not reveal primed induction of PR1. In all cases, the level of pre-established deposition of active MPK3 and MPK6 seems not to be influenced by the application of SA.

Callose deposition is another hallmark of primed immunity (Luna et al., 2011). Therefore, we sought to identify whether heightened deposition of callose also occurred upon treatment with different sulfonamides. The degree of callose deposition, shown in Figure 1C and 1D, indicates that compared with the lack of callose deposition in mock-treated (DMSO) seedlings, application of either SB, SDZ, or SMTH promotes remarkable deposition of callose in leaves. These results thus suggest that sulfonamides can function as agonists of primed immunity.

Sulfadiazine Enhances Plant Resistance to *P.s.* DC3000

Since activation of primed immunity renders sensitized plants more resistant to pathogens, we next sought to demonstrate whether treatment of full-grown plants with SDZ, as a representative member of the sulfonamide derivatives identified in the chemical screening, would confer enhanced disease resistance to the virulent pathogen *P.s.* DC3000. After different trials we observed that SDZ was most effective and reproducible if applied to grown plants as a drench through the roots. Therefore, *Arabidopsis* plants hydroponically grown using the Araponics system (http://www.araponics.com) (Supplemental Figure 1) were either mock treated with DMSO or treated with 100 μM SDZ for 3 days prior to inoculation with *P.s.* DC3000. Disease performance was assayed by measuring bacterial growth in the inoculated leaves at 0, 3, and 5 days post inoculation (dpi). Figure 2A shows that SDZ-treated plants exhibited significant reductions in bacterial growth at 3 and 5 dpi compared with DMSO-treated plants. This SDZ-mediated enhancement in resistance was not due to SDZ having an antibiotic effect against *P.s.* DC3000, since the bacteria revealed no significant alteration in its growth at concentrations of SDZ used in our experiments (Supplemental Figure 2). Lack of antibiotic effect of sulfonamides on growth of *P.s.* DC3000 was also documented by Schreiber et al. (2008) and Noutoshi et al. (2012). Therefore, the SDZ-mediated enhanced resistance in the plant is not due to a toxic effect on the growth of *P.s.* DC3000. Furthermore, in SDZ-treated plants the *PR1* gene expression was poised for increased activation upon bacterial inoculation. qRT–PCR experiments at different times post inoculation, as shown in Figure 2B, revealed notorious enhancements in *PR1* transcript accumulation in SDZ-treated plants compared with DMSO-treated plants. Thus, SDZ promotes a primed immune state in the plant for enhanced resistance to *P.s.* DC3000. Moreover, the SDZ-mediated immune response does not require intactness of the SA pathway. In fact, disease performance of *npr1* and *sid2* plants in the presence of SDZ revealed that the normal enhanced

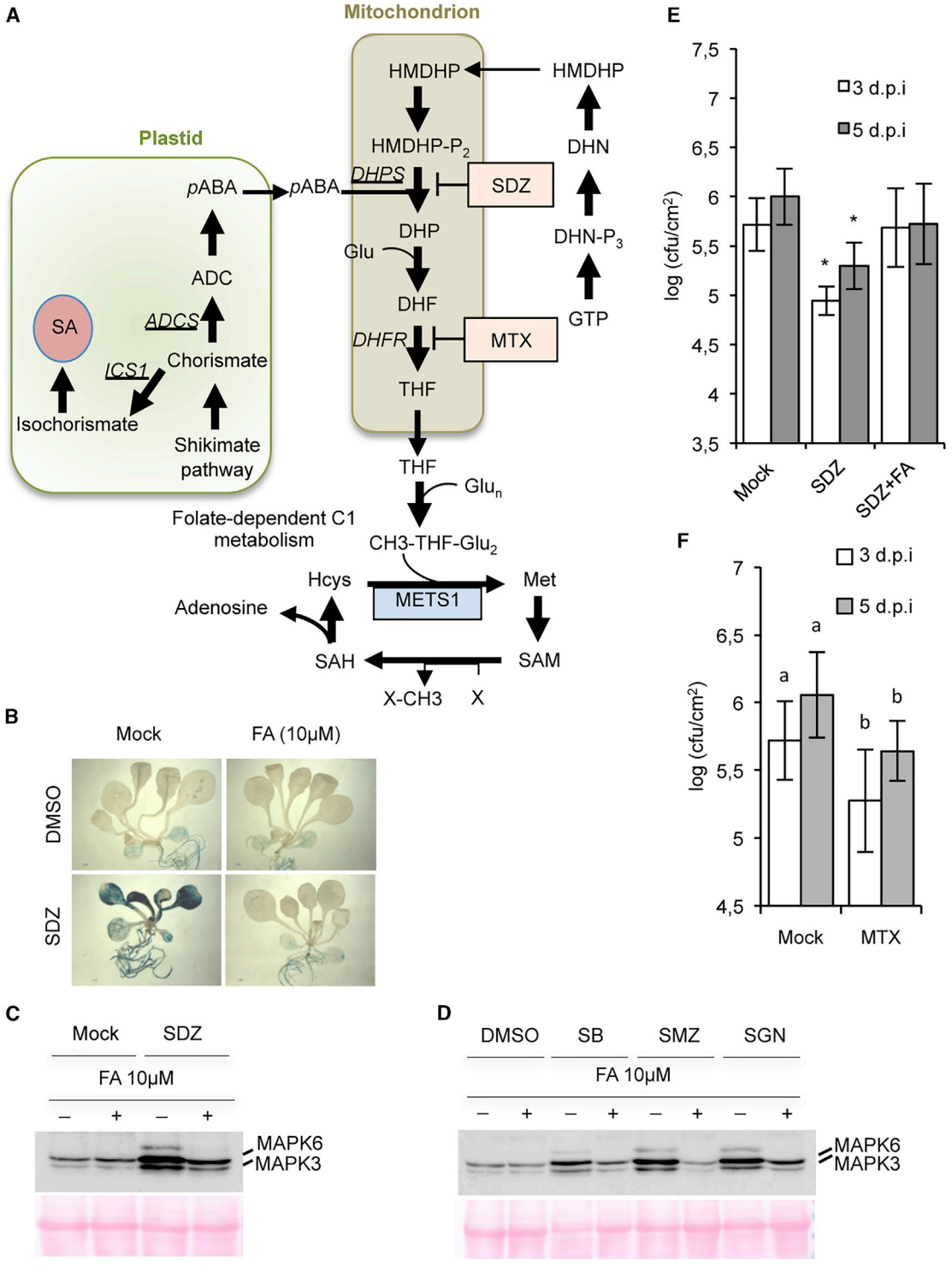

Figure 3. Folic Acid Counteracts the Effect of Sulfadiazine.

(A) The folate biosynthesis pathway in plants and the provision of methyl groups to the interconnected one-carbon (C1) metabolic pathway leading to the synthesis of *S*-adenosylmethionine (SAM). ADCS, aminodeoxychorismate (ADC) synthase (EC 2.6.1.85); *p*ABA, *p*-aminobenzoate; GTP, guanosine triphosphate; DHN, dihydroneopterin; HMDHP, 6-hydroxymethyldihydropterin; ICS, isochorismate synthase (EC 5.4.4.2); DHPS, dihydropteroate (DHP) synthase (EC 2.5.1.15); DHFR, dihydrofolate (DHF) reductase (EC 1.5.1.3); Glu, glutamate; THF, tetrahydrofolate; Hcys, homocysteine; Met, methionine; SAH, *S*-adenosylhomocysteine; METS, cobalamin-independent methionine synthase (EC 2.1.1.14).

(B) Histochemical analysis of GUS activity in *Ep5C*::*GUS* seedlings following SDZ treatment (25 μM) in the presence or absence of folic acid (FA) (10 μM). Scale bars represent 1 mm.

(legend continued on next page)

disease susceptibility of these two SA pathway-related mutants was reversed by SDZ (Figure 2C and 2D). Since *npr1* is defective in SA perception (Cao et al., 1997) and *sid2* is defective in SA biosynthesis (Wildermuth et al., 2001), our results suggest the SDZ action in promoting enhanced resistance to *P.s*. DC3000 is not under the control of the SA pathway.

Impairment of the Folate Metabolic Pathway Enhances Plant Resistance to *P.s*. DC3000

The identified sulfonamides are structural analogs of *p*-aminobenzoic acid (*p*ABA), a precursor of folate that competitively inhibits the enzyme dihydropteroate synthase (DHPS) (McCullough and Maren, 1973; Prabhu et al., 1997). This inhibition impedes the accumulation of dihydropteroic acid, the intermediate precursor of tetrahydrofolate (THF), a key step in the complex folate biosynthesis pathway (see diagram in Figure 3A). Zhang et al. (2012) demonstrated that SMZ treatment in *Arabidopsis* impairs folate metabolism and renders significant reduction in the folates pool, including THF and its derivatives. Therefore, we tested whether the sole application of folic acid (FA) could repress the SDZ-mediated transcriptional activation of *Ep5C*::*GUS*. Figure 3B shows that 10 μM FA was sufficient to revert the effect of SDZ on the transcriptional reprogramming of *Ep5C*. Moreover, the SDZ-mediated deposition of phosphorylated MAPK3 and MAPK6 was similarly reversed in the presence of FA (Figure 3C), a situation mirrored for other sulfonamides (e.g., SB, SMZ, and SGN) (Figure 3D). Likewise, FA drenching through the roots in hydroponically grown plants impaired the SDZ-mediated enhanced disease resistance to *P.s*. DC3000 (Figure 3E). These observations indicated that the sulfonamide-mediated effect on the activation of immune priming was likely due to disruption of the folate biosynthetic pathway. In fact, methotrexate (MTX), an analog of dihydrofolate that inhibits dihydrofolate reductase (Figure 3A) and perturbs the folates pool in plants (Loizeau et al., 2007, 2008), also promoted enhanced disease resistance to *P.s*. DC3000 (Figure 3F) to an extent similar to that observed for SDZ (Figure 3E). These observations sustain that a defective folate metabolic pathway is the basis for the observed sulfonamide-mediated enhanced resistance to *P.s*. DC3000.

Folic Acid Treatment Enhances Disease Susceptibility to *P.s*. DC3000

To confirm whether FA could antagonize the immune response, we inoculated *Arabidopsis* plants treated with 500 μM FA with *P.s*. DC3000. Recording of bacterial growth at 3 and 5 dpi revealed that FA promoted significant enhancements of bacterial growth (Figure 4A). This enhanced disease susceptibility to *P.s*. DC3000 was not due to a defect in the biosynthesis of SA, since SA levels following bacterial inoculation were similar in mock- and FA-treated plants (Figure 4B). Neither was sensitivity to SA abrogated by FA, since PR1-induced accumulation showed no repression during the course of *P.s*. DC3000 infection (Figure 4C). Instead, *P.s*. DC3000-induced PR1 accumulation showed a 2-fold enhancement in the FA-treated infected plants (Supplemental Figure 3) presumably as a consequence of the heightened growth of the bacteria taking place in FA-treated plants (Figure 4A). Therefore, the FA-mediated enhanced susceptibility to *P.s*. DC3000 appeared to be SA independent. Moreover, determination of transcript levels for *DHPS* and *ADCS*, encoding cardinal enzymes of the mitochondrial and the plastidial compartments, respectively, of the folate biosynthesis pathway (Figure 3A), revealed that these genes are downregulated at 48 and 72 h post inoculation (hpi) with *P.s*. DC3000 (Figure 4D). Conversely, transcript levels of *ICS1*, encoding plastidial isochorismate synthase, an enzyme of the shikimate pathway pivotal for SA biosynthesis (Wildermuth et al., 2001), were strongly upregulated following bacterial inoculation. Therefore, repression of genes of the folate pathway is encapsulated within the transcriptional reprogramming that takes place during the activation of the immune response upon *P.s*. DC3000 infection. This indicates that downregulation of the folate pathway might represent an additional layer of complexity in the control of plant immunity.

P.s. DC3000 Infection Enhances Accumulation of Methionine Synthase in *scs9* Mutants

The observed SA-independent enhanced disease susceptibility to *P.s*. DC3000 mediated by FA (Figure 4A) evokes also the SA-independent enhanced susceptibility recently described in the *SUPPRESSOR OF CSB3 9* (*scs9*) mutants (Ramirez et al., 2018). Therefore, this commonality prompted us to search in *scs9* plants for alterations in the accumulation of any protein that could give clues about this particular SA-independent susceptible phenotype. Toward this end we performed comparative proteomics analysis, under mock- and *P.s*. DC3000-inoculated conditions, between Columbia-0 (Col-0) and the two non-allelic *scs9-1* and *scs9-2* mutants. To compare relative protein abundance between genotypes and treatments, we used two-dimensional (2D) difference gel electrophoresis (DIGE). Protein extracts were differentially labeled with Cy2, Cy3, and Cy5 fluorescent dyes, and representative 2D gels are shown in Figure 5A. Only proteins that showed greater than 2.5-fold differential expression and were commonly observed in the two *scs9* allelic mutants with respect to Col-0 plants upon bacterial inoculation were selected (Supplemental Figure 4). Twenty-seven spots were selected, and proteins were identified by matrix-assisted laser desorption/ionization tandem time-of-flight mass spectrometry (MS–MALDI-TOF/TOF) and liquid chromatography–tandem mass spectrometry (LC–MS/MS) analysis. They represented 18 different proteins (Supplemental Table 1), of which 13 were highly abundant in the two *scs9* allelic lines compared with Col-0. 5-Methyltetrahydropteroyltriglutamate homocysteine methyltransferase 1 (methionine synthase [At5g17920]), hereafter named METS1, was identified in five of the selected proteins

(C and D) Western blots using anti-pTEpY antibodies of crude protein extracts from seedlings following either SDZ **(C)** or other sulfonamide (i.e., SB, SMZ, and SGN) **(D)** treatment in either the absence (−) or presence (+) of FA (10 μM).

(E) Comparative growth rate of *P.s*. DC3000 in Col-0 plants mock treated, treated with SDZ (100 μM), and treated with SDZ (100 μM) plus FA (100 μM). Asterisks indicate significant differences from mock samples (ANOVA simple test; $^*P < 0.05$).

(F) *P.s*. DC3000 growth rate in Col-0 plants following methotrexate (MTX) treatment (100 μM). Different letters indicate statistically significant different data groups related to non-treatment. Error bars indicate SD ($n = 12$ plants).

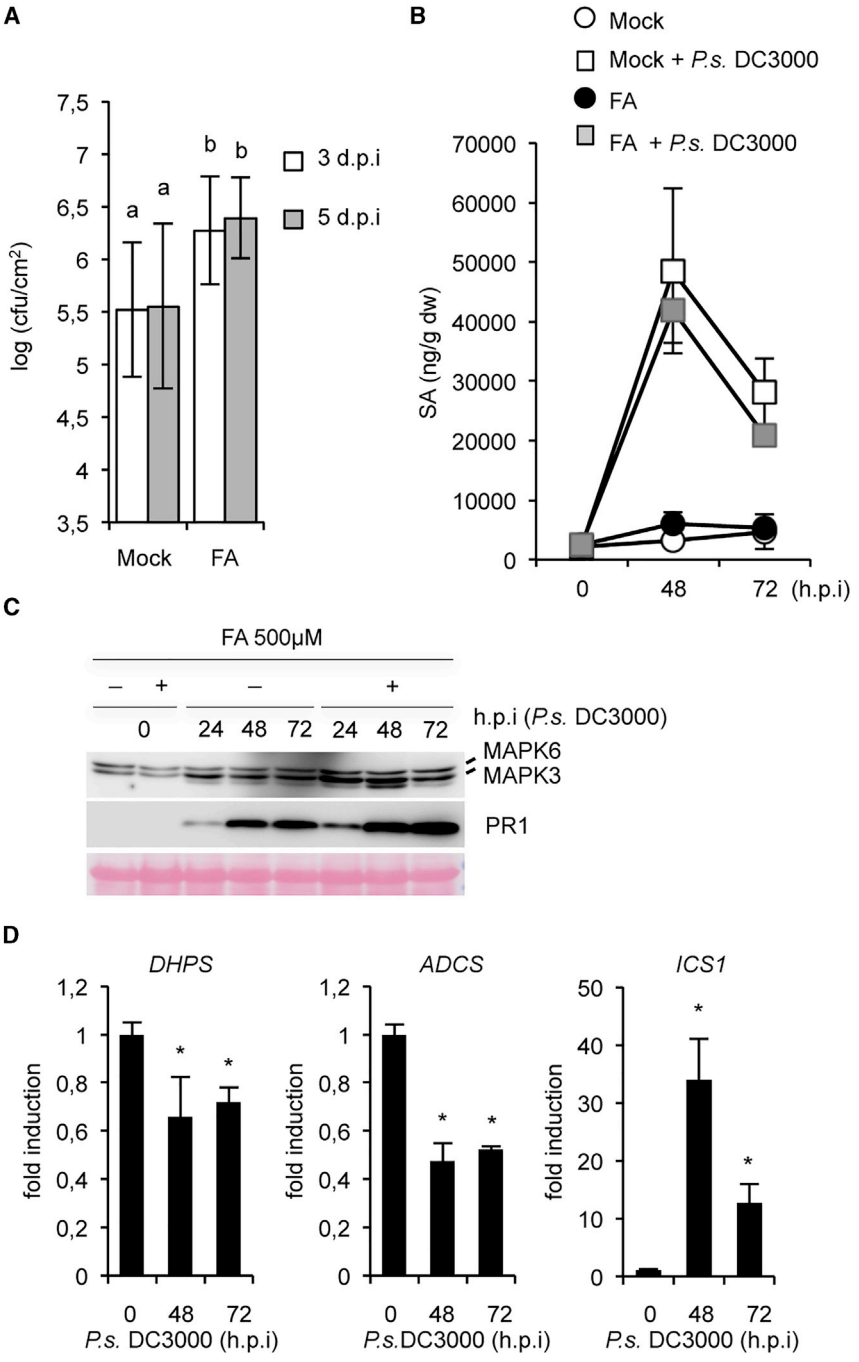

Figure 4. FA Treatment Promotes Enhanced Susceptibility toward *P.s.* DC3000.

(A) Bacterial growth rate in Col-0 plants pretreated with FA (500 µM). Error bars indicate SD (n = 12 plants). Different letters indicate statistically significant different data groups related to non-treatment control (ANOVA test; $P < 0.05$).

(B) SA content in mocked and FA-treated Col-0 plants at 0, 48, and 72 hpi with *P.s.* DC3000. Data represent mean ± SD; n = 3 replicates.

(C) Western blots of protein extracts derived from mock and *P.s.* DC3000-inoculated Col-0 plants, either treated (+) or not treated (−) with FA (500 µM). Samples were taken at 0, 24, 48, and 72 hpi with *P.s.* DC3000.

(D) qRT–PCR analysis of *DHPS*, *ADCS*, and *ICS1* gene expression in Col-0 plants at 0, 48, and 72 hpi with *P.s.* DC3000. Data represent mean ± SD; n = 3 replicates. Asterisks indicate statistically significant different data groups related to non-inoculated control plants (ANOVA test; *$P < 0.05$).

See also Supplemental Figure 3.

spots, showing stronger accumulation in *P.s.* DC3000-inoculated *scs9-1* and *scs9-2* plants compared with Col-0 (marked by arrows in Figure 5B). METS1 is a key enzyme in the 1C metabolism in which 1C units carried by the folate cofactor 5-methyl-THF-Glu2 act as methyl donors for the METS1-catalyzed synthesis of methionine (Met) in the SAM cycle (Ravanel et al., 1998, 2004) (Figure 3A). This Met is subsequently converted to SAM (Figure 3A), which acts as the universal methyl donor for methyltransferase reactions (Roje, 2006). Details of the relative abundance of METS1 protein is shown in 2D gel sectors in Figure 5B. Since the five identified METS1 spots differed in their isoelectric points (p*I*) but not so in the apparent molecular weight, their different p*I*s are likely the result of post-translational modifications of this protein. Although METS1 was one of the proteins that showed the strongest differential upregulation in *P.s.* DC3000-inoculated *scs9*-1 and *scs9-2* plants, *METS1* transcript levels, on the other hand, were not increased but instead decreased following bacterial inoculation (Figure 5C). This might suggest that increased stability of the protein or enhanced translation of the corresponding mRNA is a likely explanation accounting for the enhanced accumulation of METS1 in the *scs9* mutant plants.

Overexpression of *METS1* Enhances Disease Susceptibility to *P.s.* DC3000

We next reasoned that if the SDZ-mediated/SA-independent enhanced resistance to *P.s.* DC3000 observed in Col-0 plants (Figure 2A) is due to THF pathway inhibition, the enhanced susceptibility of *scs9* plants will be likely abrogated upon THF pathway inhibition by SDZ. Figure 6A shows that application of SDZ to *scs9-1* plants reverted the enhanced susceptibility to *P.s.* DC3000, bringing the rate of bacterial growth to levels similar to that observed in Col-0 plants. This might denote the importance of THF-dependent and METS1-mediated biosynthesis of Met for promoting enhanced susceptibility to *P.s.* DC3000. Congruently, the sole application of 1 mM Met biochemically complemented the action of SDZ and blocked the SDZ-mediated activation of *Ep5C*::*GUS* (Figure 6B) and MAP kinases setting in Col-0 seedlings (Figure 6C). All these observations reinforce the consideration of the importance of the METS1-mediated Met biosynthesis in modulating plant immunity. We next tried to corroborate these observations using *Arabidopsis* mutants defective in METS1, but failed to obtain a homozygous T-DNA insertion line in the *METS1* gene when

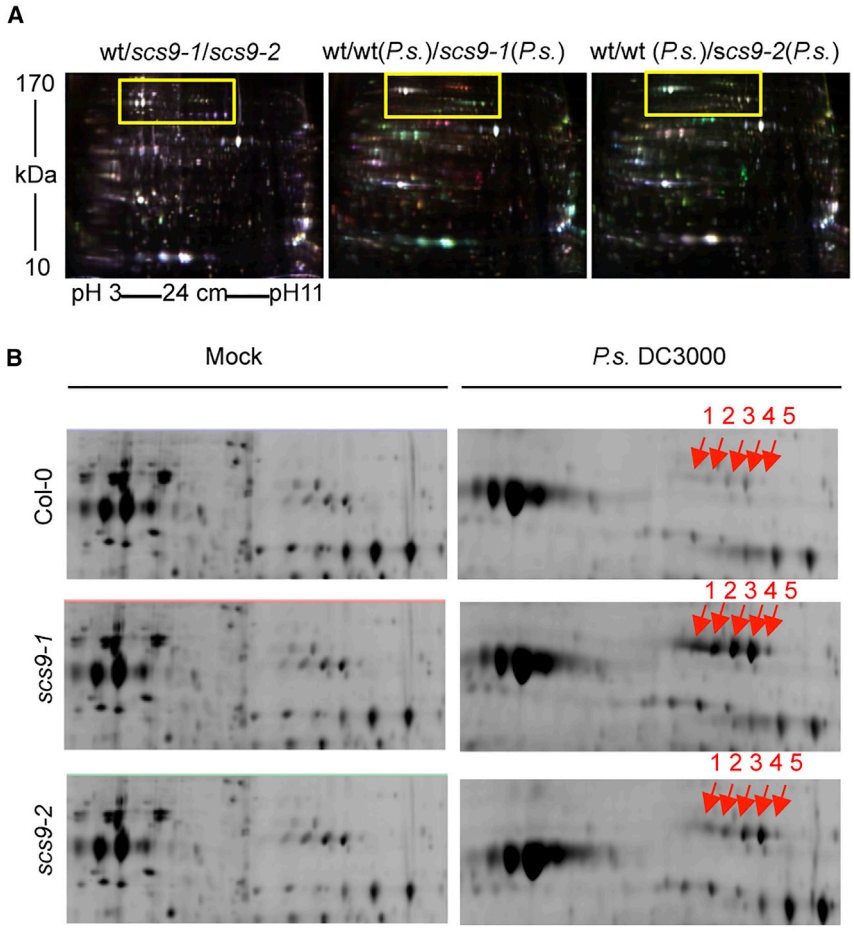

Figure 5. Comparative Proteomic Analysis of Col-0, *scs9-1*, and *scs9-2* Plants Inoculated with *P.s.* DC3000 (3 dpi).

(A) Overlay of fluorescence images for each of the 2D-DIGE gels containing proteins from mocked Col-0 (Cy2-labeled, blue), *scs9-1* (Cy5-labeled, red), and *scs9-2* (Cy3-labeled, green) plants (left); from mocked Col-0 (Cy3-labeled, green) and *P.s.* DC3000-infected Col-0 (Cy2-labeled, blue), and *scs9-1* (Cy5-labeled, red) plants (center); and from mocked Col-0 (Cy5-labeled, red) and *P.s.* DC3000-infected Col-0 (Cy2-labeled, blue), and *scs9-2* (Cy3-labeled, green) plants (right). Proteins overaccumulating in *scs9-1* appear in red, those overaccumulating in *scs9-2* appear in green, those repressed in both mutants appear in blue, and proteins showing no variation appear in white.

(B) Magnified DeCyder images, derived from the sectors marked in the 2D gels shown in **(A)** and corresponding to each of the indicated genetic backgrounds, either mocked or inoculated with *P.s.* DC3000, are shown. Different spots corresponding to the same protein (i.e., METS1) are indicated with red arrows and are tagged with their respective numbers from the list of proteins identified by MS–MALDI-TOF/TOF and LC–MS/MS (Supplemental Table 1).

(C) qRT–PCR analysis of *METS1* transcript accumulation in Col-0, *scs9-1*, and *scs9-2* plants from mock- and *P.s.* DC3000-inoculated leaves. Data represent the mean ± SD; $n = 3$ replicates.

See also Supplemental Figure 4 and Supplemental Table 1.

employing two different insertion mutants (i.e., SAIL_655_B04 [*mets1-1*] and SAIL_136_C12 [*mets1-2*]) that carry T-DNA insertions in the fourth and sixth exon, respectively (Figure 6D). In homozygosis, *mets1* mutants showed embryo lethality (Figure 6D exemplifies the phenotype of *mets1-2* mutant). Lethality in any THF pathway-defective mutant is a common theme due to the essential role played by this pathway in the cell cycle (Chen et al., 2016; Gallardo et al., 2002; Ishikawa et al., 2003). Alternatively, we asked whether heterozygous *mets1/METS1* plants might show altered disease resistance to *P.s.* DC3000 as a result of a reduced gene dosage. Figure 6E reveals that both *mets1-1/METS1* and *mets1-2/METS1* heterozygous plants support significantly less bacterial growth than homozygous *METS1/METS1* wild-type plants. Both heterozygous lines presented a significant reduction (i.e., 40%–50%) in the accumulation of the endogenous *METS1* transcripts (Figure 6F) compared with wild-type plants. This thus gives support to the hypothesis that reduced expression of *METS1* somehow facilitates activation of a more efficient immune response leading to enhanced resistance. If this is so, one could hypothesize that increased accumulation of METS1, as occurs in the infected *scs9* mutant (Figure 5B), would lead to enhanced disease susceptibility. Therefore, we asked whether the sole overexpression of *METS1* in Col-0 plants would be sufficient to promote enhancement in susceptibility toward *P.s.* DC3000 and thus mimic the *scs9* phenotype. Toward this end, we generated stable *Arabidopsis* transgenic lines expressing *METS1* (tagged with YFP) under the control of the constitutive 35S CaMV promoter (*35S::METS1-YFP* lines).

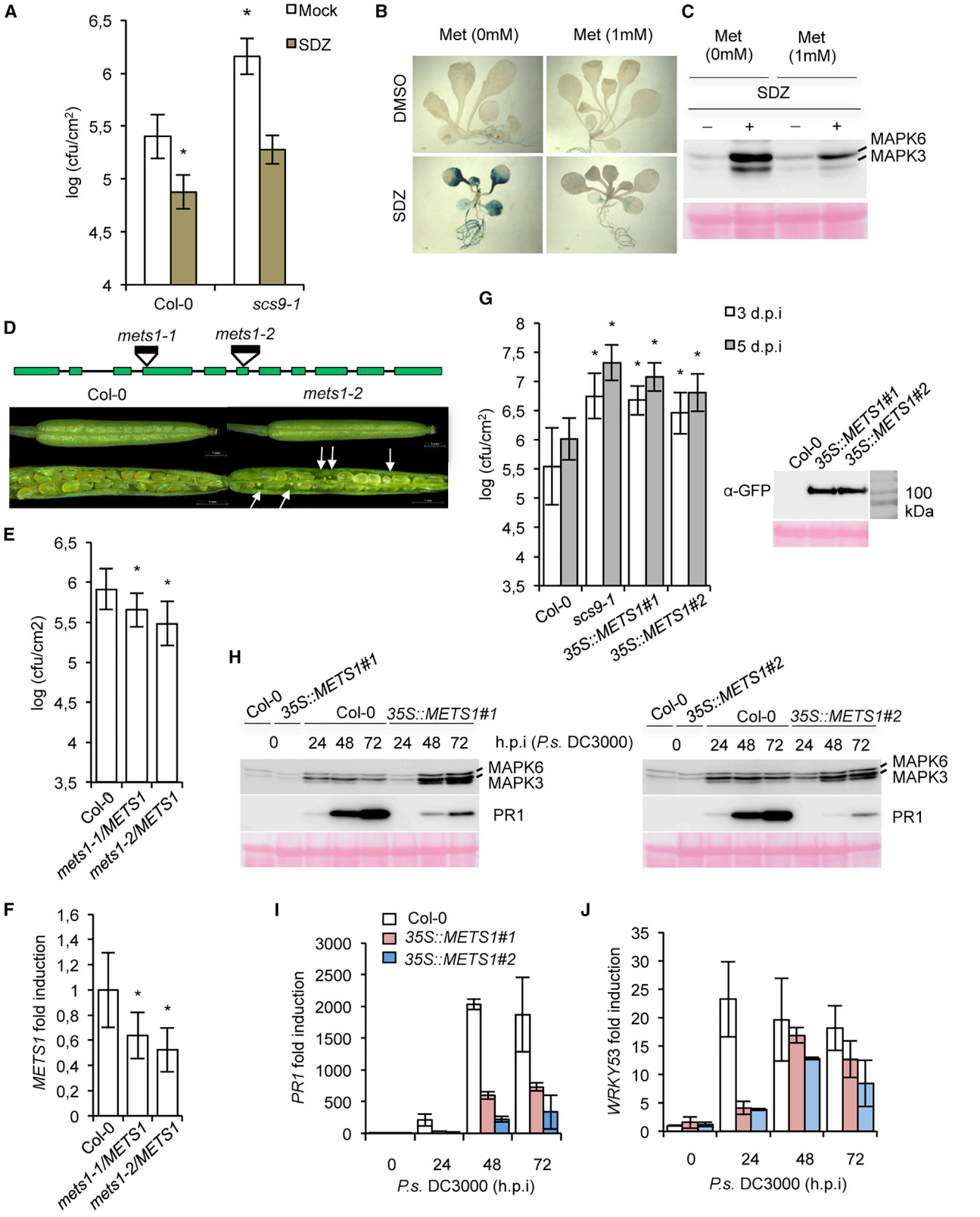

Figure 6. *METS1* Overexpression Promotes Enhanced Disease Susceptibility to *P.s.* DC3000.

(A) Bacterial growth at 3 dpi in mock- and SDZ (100 μM)-treated Col-0 and *scs9-1* plants. Error bars indicate SD (n = 12 plants). Asterisks indicate statistically significant differences related to mocked Col-0 plants (ANOVA test; *$P < 0.05$).

(legend continued on next page)

Transient expression of this construct in *Nicotiana benthamiana* revealed that METS1-YFP localizes in the cytosol, in accordance with the cytosolic ubication of 1C metabolism (Supplemental Figure 5A). The stable *Arabidopsis* transgenic plants overexpressing *METS1* did not cause any detrimental effect regarding development or plant growth (Supplemental Figure 5B), thus indicating a lack of visual phenotypic pleiotropy. Plants from two independent homozygous transgenic lines (i.e., *35S*::*METS1#1* and *35S*::*METS1#2*), showing accumulation of the fusion protein (western blot on the right of Figure 6G), were inoculated with *P.s*. DC3000 and bacterial growth recorded at 3 and 5 dpi. The susceptible *scs9-1* mutant was assayed similarly and used as a control. Results in Figure 6G revealed that the two *35S*::*METS1* lines supported significantly more bacterial growth than Col-0 plants. This enhanced susceptibility was of a magnitude similar to that attained in *scs9-1* plants. Moreover, in the two transgenic lines, deposition of phosphorylated MPK3 and MPK6 following *P.s*. DC3000 inoculation was enhanced at 48 and 72 hpi with respect to Col-0 plants (Figure 6H). This enhanced deposition of MPK kinases may reflect the enhanced signaling caused by the higher bacterial titer growing in the transgenic lines. However, and in marked contrast, the induced accumulation of the defense-related PR1 protein following *P.s*. DC3000 inoculation was dramatically repressed in both transgenic lines when compared with levels attained in control Col-0 plants (Figure 6H). Reduced accumulation of PR1 protein mirrored the reduced expression of *PR1* gene observed in the two transgenic lines following bacterial infection when compared with control Col-0 plants (Figure 6I). Furthermore, transcriptional attenuation also occurred for *WRKY53* (Figure 6J), which encodes a transcription factor pivotal for the SA-dependent transcriptional reprogramming of the immune response (Asai et al., 2002; Dong, 2004), and whose reduced expression in both *35S*::*METS1* lines was notorious at early stages of infection with *P.s*. DC3000 (Figure 6J). In summary, our results provide evidence indicating that imposed expression of METS1 dampens plant immunity to *P.s*. DC3000 and alters the transcriptional reprogramming, leading to activation of defenses.

Genome-wide DNA Methylation Enhancement Occurs in Transgenic Plants Overexpressing *METS1*

We previously identified that *P.s*. DC3000-mediated expression of *Ep5C*::*GUS* concurs with demethylation of the gene promoter region (Agorio and Vera, 2007), indicating that this marker gene is under epigenetic regulation. Moreover, constitutive expression of *Ep5C* and immune priming activation concur in RNA-directed DNA methylation (RdDM)-defective mutants (López et al., 2011). Therefore, we hypothesized that since the Met pool synthesized by METS1 through the THF-1C metabolism is the immediate precursor of SAM (Roje, 2006), the methyl donor for methyltransferases (Figure 3A), the sulfonamide-mediated promotion of *Ep5C*::*GUS* expression and enhanced resistance to *P.s*. DC3000 shown above (Figures 1 and 2) might be the result of the inhibition of DNA methylation due to impairment of the THF pathway. Under this same rationale, we hypothesized that potentiation of Met synthesis through overexpression of *METS1* may ultimately potentiate DNA methylation, promote epigenetic silencing, and consequently suppress plant immunity. To gain insight into how overexpression of *METS1* may be affecting DNA methylation on a global scale, we analyzed genome-wide DNA methylation at single-nucleotide resolution by bisulfite sequencing (BS-seq) comparatively between Col-0 and *35*::*METS1#1* plants, under both basal and *P.s*. DC3000-inductive conditions. These analyses revealed that in *35S*::*METS1#1* plants the average global DNA methylation rate (measuring the methylation ratio in all cytosine contexts) was 20.6% higher than in Col-0 plants (Figure 7A). The strongest effect on methylation occurred in the CHH context, which increased by 33.3% relative to Col-0, followed by CHG and CG methylation contexts with 13.2% and 5.7% increases, respectively (Figure 7A). The comparison of methylation overview plots between Col-0 and *35S*::*METS1#1* plants revealed that DNA methylation rate, in all sequence contexts, was increased in the transgenic line across the entire genome (Figure 7B). However, methylation differences between both genotypes were more prominent over the pericentromeric regions (rich in repetitive sequences and transposable elements [TEs]) in the five chromosomes of *Arabidopsis* (Figure 7B), which in fact are hot methylation spots in *Arabidopsis* (Zhang et al., 2006). This pericentromeric-based enrichment in methylation agrees with major enhancement of methylation observed in CHH and CHG contexts, since CG-context methylation is rare in TEs in *Arabidopsis* (Cokus et al., 2008). Accordingly, average methylation levels over TEs were strongly increased in *35S*::*METS1#1* plants, especially in CHG and CHH contexts (Figure 7C). Methylation was also increased, but more moderately, over protein-coding genes (PCGs) in

(B) Inhibition of the SDZ-mediated induction of *Ep5C*::*GUS* expression in seedlings following a combined treatment of SDZ with methionine (Met). Scale bars represent 1 mm.
(C) Western blot using anti-pTEpY antibodies of crude protein extracts from seedlings treated with SDZ in either the presence or absence of 1 mM methionine.
(D) Embryonic lethality of *mets1* mutants. Two allelic mutants from T-DNA insertion lines were studied. Position of T-DNA insertion (black rectangle) is represented in a diagram of the *METS1* gene (At5g17920). Comparison between a representative silique from Col-0 and the *mets1* mutant is shown. Scale bars represent 1 mm. A quarter of the total seeds in *mets1* were devoid of a functional embryo (indicated by white arrows).
(E) Comparative *P.s*. DC3000 growth in heterozygous mutants (*mets1-1* and *mets1-2*) related to Col-0 plants.
(F) qRT–PCR analysis of *METS1* gene expression in non-inoculated Col-0, *mets1-1/METS1*, and *mets1-2/METS1* plants. Data represent mean ± SD; $n = 3$ replicates. Asterisks indicate statistically significant differences related to Col-0 plants (ANOVA test; $^*P < 0.05$).
(G) Comparative *P.s*. DC3000 growth in Col-0, *scs9-1* and two independent *35S*::*METS1* overexpressing lines (lines #1 and #2). Error bars indicate SD ($n = 12$ plants). Asterisks indicate statistically significant differences related to Col-0 plants (ANOVA test; $^*P < 0.05$) The inset shows a western blot, developed with anti-GFP antibodies, showing the accumulation of the fusion METS1-YFP protein in the two independent transgenic lines.
(H) Western blots of protein extracts from Col-0, *35S*::*METS1#1*, and *35S*:: *METS1#2* plants at 0, 24, 48, and 72 hpi with *P.s*. DC3000. Western blots were developed using anti-pTEpY and anti-PR1 antibodies.
(I and J) qRT–PCR analysis of *PR1* **(I)** and *WRKY53* **(J)** gene expression in Col-0, *35S*::*METS1#1*, and *35S*::*METS1#2* plants at 0, 24, 48, and 72 hpi with *P.s*. DC3000. Data represent mean ± SD; $n = 3$ replicates.
See also Supplemental Figure 5.

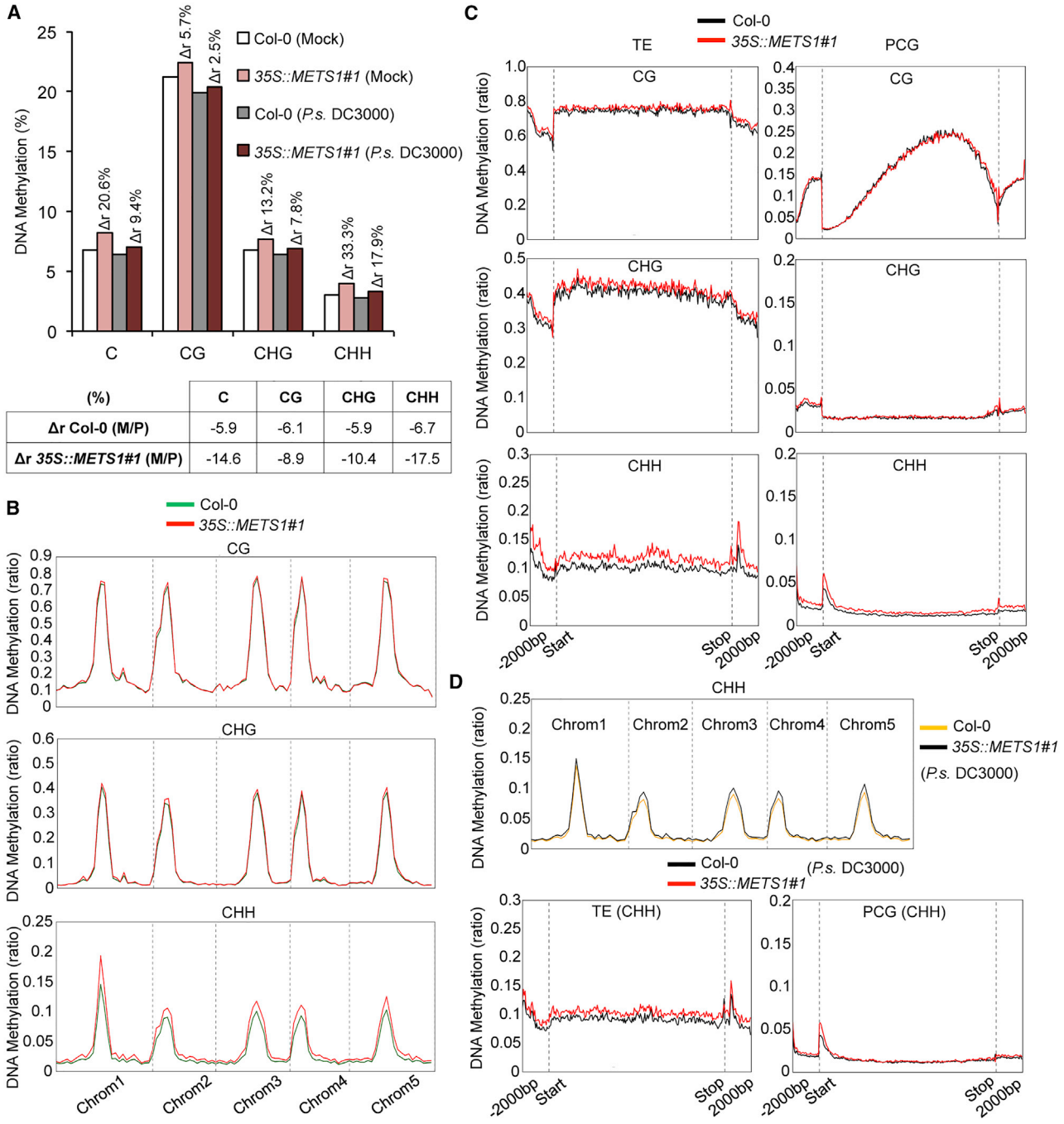

(%)	C	CG	CHG	CHH
Δr Col-0 (M/P)	-5.9	-6.1	-5.9	-6.7
Δr *35S::METS1#1* (M/P)	-14.6	-8.9	-10.4	-17.5

Figure 7. *METS1* Overexpression Promotes Genome-wide DNA Methylation Enhancement.

(A) Comparative analysis of average genome-wide DNA methylation rate (%) between Col-0 and *35S*::*METS1* plants in both mock and *P.s.* DC3000-inoculated plants. Percentage variation in cytosine methylation rate at the whole-genome level (C) or in the three distinct methylation contexts (i.e., CG, CHG, and CHH) is shown. Δr denotes the percentage variation in methylation rate (%) in *35S*::*METS1#1* plants compared with Col-0, and in the table below that observed in mocked (M) Col-0 and *35S*::*METS1#1* plants when compared with *P.s.* DC3000-inoculated plants (P).

(B) Comparative DNA methylation-level overview plots across the five chromosomes of the *Arabidopsis* genome for the three sequence contexts (i.e., CG, CHG, and CHH) between non-inoculated Col-0 and *35S*::*METS1* plants. Note that major differences are observed within the CHH methylation context.

(C) Comparative average methylation-level diagram of TEs and PCGs in the CG, CHG, and CHH sequence contexts between non-inoculated Col-0 and *35S*::*METS1* plants.

(D) Comparative DNA methylation-level overview plot across the five chromosomes of the *Arabidopsis* genome for the CHH methylation context, and average methylation-level diagram of TEs and PCGs for the CHH methylation context between Col-0 and *35S*::*METS1* plants at 72 hpi with *P.s.* DC3000. See also Supplemental Figures 6 and 7.

35S::*METS1#1* plants (Figure 7C). Therefore, overexpression of THF-dependent *METS1* exerts a "methylation pressure" over the entire genome that results in an enhanced methylation rate, particularly in pericentromeric regions.

P.s. DC3000-Induced Demethylation in Col-0 and *35S*::*METS1* Plants

In accordance with previous studies (Dowen et al., 2012; Pavet et al., 2006), we observed that *P.s.* DC3000 infection promoted a reduction in DNA methylation level in all sequence contexts in Col-0 (Figure 7A and Supplemental Figure 6). This bacterial-induced demethylation occurred also in *35S*::*METS1#1* plants (Figure 7 and Supplemental Figure 6) and was even stronger than that observed in Col-0 (table inset in Figure 7A). This differential reduction between genotypes is likely explained by the higher methylation status observed under basal conditions in *35S*::*METS1#1* plants. Nevertheless, and despite this *P.s.* DC3000-mediated global reduction in methylation levels and the higher bacterial titers attained in *35S*::*METS1#1* plants (Figure 6G), the *35S*::*METS1#1* plants still retained a 9.4% enhancement in DNA methylation over Col-0 plants upon bacterial inoculation (Figure 7A and 7D; Supplemental Figure 7A and 7B). Methylation-rate differences between infected genotypes were most pronounced in a CHH context (17.9%), but measurable differences were also retained in a CHG context (7.8%) and to a lesser extent also in a CG (2.5%) context (Figure 7A). The sustained enhanced methylation status that is still retained after bacterial infection in *35S*::*METS1#1* plants in comparison with infected Col-0 plants remained over the five chromosomes of *Arabidopsis*, with major differences observed in pericentromeric regions, and in particular in TE in the CHH methylation context (Figure 7D). This was also observed for the status of DNA methylation in a CHG context (Supplemental Figure 7A and 7B) and more marginally in the case of a CG context (Supplemental Figure 7A and 7B). The sustained enhanced genome-wide DNA methylation observed in *35S*::*METS#1* plants after bacterial infection also occurred in *35S*::*METS1#2*-infected plants (Supplemental Figure 7C). For the later transgenic line, as observed for the former line, the sustained hypermethylation status compared with Col-0 plants following *P.s.* DC3000 infection remained over the five chromosomes, was more prominent in pericentromeric regions, and was clearly enhanced in the CHH methylation context of both TE and PGC genomic regions (Supplemental Figure 7C). Thus, in accordance with the DNA methylation remodeling process set in motion during the activation of the immune response toward *P.s.* DC3000 (Pavet et al., 2006; Dowen et al., 2012), the genome-wide "methylation pressure" promoted by the overexpression of *METS1* appears to counteract the general DNA demethylation process activated upon *P.s.* DC3000 infection, which in turn may be dampening the plant immune response as occurs in *35S*::*METS1* plants (Figure 6G). Our results thus contribute to a better understanding of the epigenetic control of plant immunity, and highlight the THF-dependent 1C metabolism as a new layer of complexity for the modulation of this adaptive response.

DISCUSSION

Here we identified different sulfonamides promoting primed immunity in *Arabidopsis*. Sulfonamides competitively inhibit DHPS, an essential enzyme of the folate pathway, and block the accumulation of dihydropteroic acid, which is the precursor of tetrahydrofolate (THF) (Prabhu et al., 1997). The inhibition of the essential THF pathway by sulfonamides signals a mechanism leading to the activation of the methylation-sensitive *Ep5C*::*GUS* gene as well as the accumulation of MPK3 and MPK6 and deposition of the defense-related cell wall polymer callose, which are hallmarks of immune priming activation (Martínez-Medina et al., 2016; Mauch-Mani et al., 2017). This priming status triggered by sulfonamides was not associated with the constitutive expression of SA-responsive genes. According to Beckers et al. (2009) and Conrath et al. (2015), pre-establishment of cell priming, and consequently of induced resistance, is an evolutionary phenomenon whereby cells become sensitized to respond faster and/or stronger to a pathogenic insult. We revealed that sulfonamide treatment sensitized plants for enhanced accumulation of the defense-related and SA-responsive PR1 marker following SA application or *P.s.* DC3000 infection. This thus reinforces the notion that blocking the THF pathway initiates signaling for immune priming activation. Therefore, the present finding identifies a point through which primary metabolism (i.e., THF metabolism) can modulate immune responses. Since the *Arabidopsis* genome contains two isoforms of DHPS (Storozhenko et al., 2007), treatment with sulfonamides very likely would promote a phenotype analogous to a double-knockdown mutation, and thus served to uncover a new role of the THF pathway in modulating plant immunity. Previous studies have similarly identified that sulfonamides exert a positive effect on disease resistance and pathogen-induced cell death (Schreiber et al., 2008; Noutoshi et al., 2012). However, the exact molecular mechanism as to how sulfonamides promoted these phenotypes was not clarified. Interestingly, our results indicate that the resistance phenotype conferred by the inhibition of the THF pathway appears to operate downstream and/or independent of the SA pathway. This conclusion was drawn through the observation that the disease resistance-promoting effect of SDZ still remains effective when assayed in *npr1* and *sid2* mutants defective in SA perception and biosynthesis, respectively (Cao et al., 1997; Wildermuth et al., 2001). Furthermore, our findings also invoke the existence of a repressive effect of the THF pathway toward plant immunity, as the implementation of the pathway by the pharmacological application of FA to Col-0 plants enhanced susceptibility to *P.s.* DC3000, and this effect occurs without impairing the synthesis or perception of SA. Moreover, downregulation of marker genes of the THF pathway concurs with activation of the defense-responsive genes during the course of *P.s.* DC3000 infection, further sustaining that circumstantial downregulation of the THF pathway is encapsulated within the immune-related transcriptional reprogramming. All these results thus point toward a critical role of the THF pathway in modulating plant immune responses.

The SA-independent enhanced susceptibility to *P.s.* DC3000 promoted by FA evokes the phenotype of the recently described *scs9* mutants of *Arabidopsis*, which are defective in a tRNA methyltransferase mediating 2′-*O*-ribose methylation of selected tRNAs (Ramirez et al., 2018). This similarity prompted us to search in *scs9* plants for factors determining susceptibility through a comparative proteomic approach, which allowed us to identify METS1 protein overaccumulating in the *scs9* mutants following *P.s.* DC3000 inoculation when compared

with wild-type plants. METS1 is in charge of the synthesis of Met within the recirculating SAM cycle of the THF-dependent 1C metabolism (Figure 3A), where the methyl units carried by folate cofactors (5-methyl-THF derivative) act as methyl donors for the METS1-catalyzed synthesis of Met (Figure 3A) (Ferrer et al., 2004). Newly synthesized Met is converted to SAM (Giovanelli et al., 1985), which is the universal methyl group donor utilized by most methyltransferases to methylate DNA, RNA, and histones and other proteins (Loenen, 2006). Therefore, we hypothesized that the induced overaccumulation of METS1 in *P.s*. DC3000-infected *scs9* mutants may be pivotal in promoting SA-independent disease susceptibility. This was subsequently corroborated upon the observation that disease susceptibility to *P.s*. DC3000 is promoted in *35S::METS1* plants, thus allowing to hypothesize that THF pathway/1C metabolism might negatively regulate plant immunity. This consideration can be further substantiated if we consider that reduced expression of *METS1*, as observed in non-lethal heterozygous *mets1/METS1* plants, leads to enhanced disease resistance to *P.s*. DC3000.

Zhang et al. (2012) identified the sulfonamide SMZ as a chemical suppressor of epigenetic gene silencing in *Arabidopsis*. SMZ-treated plants exhibited substantial reduction in global DNA methylation, indicating that sulfonamides confer epigenetic regulation via impairment of THF-dependent methyl supplies. Likewise, release of epigenetic gene silencing was similarly observed in plants treated with methotrexate (Loizeau et al., 2008; Zhang et al., 2012). Moreover, inhibition of SAHH1 (*S*-adenosylhomocysteine hydrolase), an enzyme of the 1C metabolism in charge of the conversion of SAH to homocysteine, the precursor of Met in the SAM cycle (Figure 3A), similarly releases epigenetic gene silencing by promoting reduction in the level of DNA methylation (Rocha et al., 2005). More recently, Zhou et al. (2013) identified folylpolyglutamate synthase (FPGS1), mediating polyglutamylation of folates for their disposal to the METS1 enzyme to synthesize Met (Figure 3A), as a critical factor for genome-wide DNA methylation and gene silencing. Also, Groth et al. (2016) identified the hypomorphic mutant *mthfd1-1*, which is defective in MTHFD1 (methylenetetrahydrofolate dehydrogenase/methenyltetrahydrofolate cyclohydrolase) activity, required for the interconversion of THF species in the 1C metabolism for Met synthesis via METS1, as carrying genome-wide hypomethylation and TE derepression. Moreover, we previously reported that a normal functioning of the RdDM epigenetic pathway is required for disease susceptibility, and when this pathway is defective primed immunity is activated (López et al., 2011), thus uncovering the importance of epigenetic control as an additional layer of complexity in the regulation of plant immunity. All these observations support interweaving of the THF/1C metabolism and epigenetic mechanisms for the final shaping of plant immunity. In fact, our finding that imposed expression of *METS1* results in a genome-wide global enhancement of DNA methylation and concurs with enhancement in disease susceptibility to *P.s*. DC3000, gives further support to the idea that the THF pathway and DNA methylation mechanisms are interlinked biochemical processes controlling, to some extent, plant immune responses and disease resistance. The imposed hypermethylation status mediated by overexpression of *METS1* might antagonize, or slow down, the release of the silencing status though DNA demethylation upon demand (e.g., following pathogen attack), thus affecting gene expression. In fact, the imposed hypermethylation status might result in depressed expression of key genes involved in adaptive responses, a situation that was in fact observed in the *35S::METS1* plants for the SA-marker genes following *P.s*. DC3000 infection.

Thus, the fine-tuning of DNA methylation status controlled by the metabolic flux of the THF/1C metabolism may be the key for the shaping of an effective immune response and might serve to illustrate the importance of this metabolic pathway for flexible adaptation of plants to changes in the environment, and in particular to pathogen attack. Identification of specific regions of the genome particularly sensitive to this control during the immune response is our challenge for the future.

METHODS

Plant Material and Growth Conditions

Arabidopsis thaliana plants were grown in growth chambers (19°C–22°C, 10 000 lux fluorescent illumination) on a 10-h light/14-h dark cycle. All mutants and transgenic plants are in Col-0 background. T-DNA insertion mutants and primers used to identify insertions by PCR are listed in Supplemental Table 2.

Chemical Genetic Screening

Three sterilized and stratified seeds per well were sown in multiwell plates with 100 μl of half-strength Murashige and Skoog solid medium (supplemented with 0.5% saccharose and 0.01% 2-(*N*-morpholino)ethanesulfonic acid), with or without 25 μM (dissolved in DMSO) of each of the individual compound present in the LATCA library. Histochemical analysis of GUS activity was analyzed as previously described (Coego et al., 2005) on 7-day-old treated seedlings. Positive hits were reconfirmed using at least 100 seedlings.

Plant Treatments

Seven-day-old seedlings germinated on solid Murashige and Skoog were transferred to 7 mL of liquid Murashige and Skoog medium containing each of the indicated compounds and kept for 7 days with soft orbital shaking (90 rpm) in multiwell plates. For determination of callose deposition, treated seedlings were stained with aniline blue and analyzed with epifluorescence microscopy, and callose deposition quantifications were performed as previously described (Dobón et al., 2015). For FA or Met complementation assays of SDZ-mediated effect, compounds were applied together with sulfonamides. Full-grown plants (4 weeks old) grown in soil were treated with FA (500 μM) or MTX (100 μM) by immersion for 20 s in 250 mL of each solution and after 3 days the plants were inoculated with *P.s*. DC3000. For hydroponically grown plants, seeds were sown on Agargel 0.6% in Araponics holders, and plants were grown for 4 weeks with weekly changes of the irrigation solution. Treatments with chemicals were performed by drenching through the roots at the indicated concentration during 3 days previous to the inoculation with *P.s*. DC3000.

Analysis of Antibiotic Effect of SDZ on *P.s*. DC3000

P.s. DC3000 liquid cultures were prepared in a concentration of 10^3 and 10^2 cells/mL. One hundred microliters of each culture was plated on solid Luria–Bertani medium, with or without SDZ (100 μM), and colony-forming units (CFU) were quantified as previously described (Pato and Brown, 1963).

Pseudomonas syringae DC3000 Inoculations

Arabidopsis leaves of 4-week-old plants were inoculated with *P.s*. DC3000 as previously described (Ramírez et al., 2013) using a bacterial inoculum of a final OD_{600} of 0.1, with 0.02% Silwet L-77 (Crompton Europe) if inoculated by spray, or with a further 1/500 dilution (without

Silwet L-77) when inoculation was performed by leaf infiltration with a syringe. Inoculated leaves were sampled at the indicated times to quantify bacterial growth rate, represented as mean ± SD of log CFU/cm^2 from 12 plants for each data point. $MgSO_4$ (10 mM) was used as control solution (mock). Unless otherwise indicated, inoculations were performed by leaf infiltration.

qRT–PCR

qPCRs were performed using a 7500 Fast Real-Time PCR System detection system (7500 Software v2.0) and SYBR-Green reagent (Power PCR Master Mix, Applied Biosystems) as described previously (García-Andrade et al., 2013). One microgram of RNA (purified by DNA-free Ambion kit; Invitrogen) was used for reverse transcription. Primers used are listed in Supplemental Table 2. *ACTIN2* or *SAND* was used as reference gene.

Western Blots

Protein extraction, SDS–PAGE, and immunoblotting were performed as previously described (Dobón et al., 2015).

Determination of SA Level

SA was extracted and quantified by high-performance liquid chromatography as previously described (Camañes et al., 2012).

Protein Labeling, 2D Electrophoresis, Gel Imaging and Data Analysis, and MS–MALDI-TOF/TOF and/or LC–MS/MS Analyses

Five-week-old plants were spray-inoculated with *P.s*. DC3000 and leaves were sampled at 3 dpi. One gram of frozen leaf tissue was extracted with 1 mL of phosphate–citrate buffer (84.4 mM citric acid and 31.2 mM Na_2HPO_4). Total protein was measured with the Bradford reagent using BSA as standard control. One hundred micrograms of protein was precipitated with 1 volume of 20% tricarboxylic acid for 2–3 h at 4°C and the pellet further washed with acetone. Proteins were dissolved in lysis buffer (7 M urea, 2 M thiourea, 4% CHAPS, 20 mM Tris–HCl [pH 8.5]) for 2D DIGE analysis. Protein samples were labeled using the CyDyes DIGE fluorescent dyes (Cy2, Cy3, and Cy5) according to the manufacturer's instructions (GE Healthcare). Each sample (50 μg) was then mixed with 40 μL of isoelectrofocusing (IEF) rehydration buffer (8 M urea, 4% CHAPS, 0.005% bromophenol blue) containing 65 mM dithiothreitol (DTT) and 1% IPG buffer (pH 3–11), and loaded on the gel, making one gel per each biological replicate. IEF was performed on an IPGphor unit (GE Healthcare) as described by Gerber et al. (2008). Each IEF strip was equilibrated separately for 15 min in 10 mL of equilibration solution I (0.05 M Tris–HCl buffer [pH 8.8] containing 6 M urea, 30% glycerol, 2% SDS, and 200 mg DTT per 10 mL of buffer) followed by equilibration solution II (substituting DTT for 250 mg of iodoacetamide per 10 mL of buffer and adding 0.01% bromophenol blue) before being applied directly to the second-dimension 12.5% SDS–PAGE gels. After SDS–PAGE, CyDye-labeled proteins were visualized by fluorescence scanning using a Typhoon Trio scanner (GE Healthcare) with the wavelengths corresponding to each CyDye. Cy2 images were scanned using a blue laser (488 nm) and a 520-nm bandpass (BP) 40 emission filter. Cy3 images were scanned using a green laser (532 nm) and a 580-nm BP 30 emission filter. Cy5 images were scanned using a red laser (633 nm) and a 670-nm BP 30 emission filter. All gels were scanned at 200-μm pixel size resolution. Image gel analysis was carried out using the DeCyder 2D Software V6.5 (GE Healthcare). Protein spots that showed a statistically significant change in abundance of at least 2.5-fold between control and *P.s*. DC3000-infected material using a Student's *t*-test ($P < 0.05$) were considered as being differentially expressed. For picking spots of interest, CyDye gels were stained using the Protein Silver Staining Kit (GE Healthcare). Proteins were excised using an Ettan Spot Picker (GE Healthcare), and destained with two 5-min washes with acetonitrile (/H_2O (1:1, v/v), followed by rehydration with 50 mM ammonium bicarbonate for 5 min and 25 mM ammonium bicarbonate in 50% (v/v) ACN for 15 min. Gel pieces were then manually digested with sequencing-grade trypsin (Promega) and subjected to MS–MALDI-TOF/TOF and LC–MS/MS analyses in the SCSIE_University of Valencia Proteomics Unit, a member of ISCIII ProteoRed Proteomics Platform. Proteins were identified with a confidence ≥95%, using Swiss-Prot as search database.

Gene Constructs

The *METS1* cDNA (At5g17920) coding sequence was cloned by using the Expand High Fidelity PCR kit (Roche) and the specific primers *BP-FW* and *BP-Rv* fused with Gateway adaptors. Using Gateway technology (Life Technologies), it was recombined to *pDONR207* using the BP ClonaseMixII kit (Invitrogen), and then into the destination vector *pEarleyGate101* (*YFP* in C-terminal) using an LR ClonaseMixII kit (Invitrogen). Primers used in the cloning process are listed in Supplemental Table 2. The *PIP1-mCherry* construct was obtained from Dobón et al. (2015). The *METS1-YFP* construct was introduced into Col-0 plants by *Agrobacterium*-mediated plant transformation to generate stable transgenic lines.

Transient Expression in *N. benthamiana* and Confocal Laser-Scanning Microscopy

Fully expanded leaves of *N. benthamiana* were infiltrated with a suspension of *Agrobacterium tumefaciens* C58 bearing the relevant construct at OD_{600} = 1, and this plant tissue was analyzed 3–4 days thereafter with a Zeiss 780 microscope. For YFP detection, samples were excited with an argon 488-nm laser line, and a fluorescence emission window of 30 nm centered at 515 nm. For detection of mCherry, a laser line at 561 nm was used for excitation and fluorescence emission was analyzed from 595 to 629 nm. Images analyses were processed with ZEN 2011 software.

Genome-wide DNA Methylation-Level Analysis by BS-Seq

Methylation analysis was carried out with 80 ng of genomic DNA extracted from leaves. Three biological replicates were conducted per genotype and treatment. DNA was used for methylC-seq library preparation as described by Urich et al. (2015). Following bisulfite conversion and purification, adapter-ligated DNA molecules were sequenced using Illumina HiSeq in the Methyl MaxiSeq Epigenetic service (Zymo Research [ZR], Irvine, CA). Reads were analyzed using the ZR analysis pipeline and using Bismark as the alignment software, allowing single cytosine methylation measurements resolution. The methylation level of each sampled cytosine for each sequence context was estimated as the number of reads reporting a C, divided by the total number of reads reporting a C or T. Fisher's exact test or Student's *t*-test was performed for each cytosine with a minimum coverage of five aligned sequence reads to identify statistically significant methylation differences. DNA methylation rate in each context was determined as the average of the methylation ratio of all cytosines belonging to each context. DNA methylation rate by chromosome across the whole genome was represented as the average of the methylation level of all cytosines from each context localized in each bin. The whole genome was divided into 100 bins. For PCG and TE plots, methylation ratio was represented as the average of the methylation level of all cytosines found in each bin. All PCGs and TEs were divided into 200 bins.

ACCESSION NUMBERS

The authors declare that all data generated and/or analyzed, supporting the results of this research, are available within the manuscript and its Supplemental Information section. The data discussed in this publication on genome-wide DNA methylation-level analysis in Col-0 plants and in Col-0 plants overexpressing *METS1* have been deposited in the NCBI Gene Expression Omnibus and are accessible through series accession number GEO: GSE128768.

SUPPLEMENTAL INFORMATION

Supplemental Information is available at *Molecular Plant Online*.

FUNDING

The authors have no funding to report concerning this study.

AUTHOR CONTRIBUTIONS

B.G. performed the experiments. B.G. and P.V. designed the experiments and analyzed the data. P.V. wrote the article. Both authors supervised the written manuscript.

ACKNOWLEDGMENTS

We acknowledge V. Flors for the determination of SA level, S. Tárraga for the 2D-DIGE analysis and selection of spots proteins, and the SCSIE_University of Valencia Proteomics Unit for MS–MALDI-TOF/TOF and/or LC–MS/MS analyses. We thank J. Forment for his assistance with the analysis of methylation data from the ZR platform, and J. García-Andrade, V. Ramirez, and L. Castelblanque for critical discussions. No conflict of interest declared. We acknowledge the Spanish Ministerio de Ciencia, Innovacion y Universidades (MICIU) for grants BFU2015-68199-R RTI2018-098501-B-100 to P.V.

Received: October 3, 2018
Revised: March 26, 2019
Accepted: April 23, 2019
Published: May 8, 2019

REFERENCES

Agorio, A., and Vera, P. (2007). ARGONAUTE4 is required for resistance to *Pseudomonas syringae* in *Arabidopsis*. Plant Cell **19**:3778–3790.

Ahuja, I., Kissen, R., and Bones, A.M. (2012). Phytoalexins in defense against pathogens. Trends Plant Sci. **17**:73–90.

Asai, T., Tena, G., Plotnikova, J., Willmann, M.R., Chiu, W.L., Gomez-Gomez, L., Boller, T., Ausubel, F.M., and Sheen, J. (2002). MAP kinase signalling cascade in *Arabidopsis* innate immunity. Nature **415**:977–983.

Beckers, G.J., Jaskiewicz, M., Liu, Y., Underwood, W.R., He, S.Y., Zhang, S., and Conrath, U. (2009). Mitogen-activated protein kinases 3 and 6 are required for full priming of stress responses in *Arabidopsis thaliana*. Plant Cell **21**:944–953.

Berger, S., Papadopoulos, M., Schreiber, U., Kaiser, W., and Roitsch, T. (2004). Complex regulation of gene expression, photosynthesis and sugar levels by pathogen infection in tomato. Physiol. Plant. **122**:419–428.

Bilgin, D.D., Zavala, J.A., Zhu, J., Clough, S.J., Ort, D.R., and DeLucia, E.H. (2010). Biotic stress globally downregulates photosynthesis genes. Plant Cell Environ. **33**:1597–1613.

Bolton, M.D. (2009). Primary metabolism and plant defense—fuel for the fire. Mol. Plant Microbe Interact. **22**:487–497.

Camañes, G., Pastor, V., Cerezo, M., García-Andrade, J., Vicedo, B., García-Agustín, P., and Flors, V. (2012). A deletion in NRT2.1 attenuates pseudomonas syringae-induced hormonal perturbation, resulting in primed plant defenses. Plant Physiol. **158**:1054–1066.

Cao, H., Glazebrook, J., Clarke, J.D., Volko, S., and Dong, X. (1997). The *Arabidopsis* NPR1 gene that controls systemic acquired resistance encodes a novel protein containing ankyrin repeats. Cell **88**:57–63.

Chen, Y., Zou, T., and McCormick, S. (2016). S-adenosylmethionine synthetase 3 is important for pollen tube growth. Plant Physiol. **172**:244–253.

Coego, A., Ramirez, V., Ellul, P., Mayda, E., and Vera, P. (2005). The H_2O_2-regulated Ep5C gene encodes a peroxidase required for bacterial speck susceptibility in tomato. Plant J. **42**:283–293.

Cokus, S.J., Feng, S., Zhang, X., Chen, Z., Merriman, B., Haudenschild, C.D., Pradhan, S., Nelson, S.F., Pellegrini, M., and Jacobsen, S.E. (2008). Shotgun bisulphite sequencing of the *Arabidopsis* genome reveals DNA methylation patterning. Nature **452**:215–219.

Conrath, U., Beckers, G.J., Langenbach, C.J., and Jaskiewicz, M.R. (2015). Priming for enhanced defense. Annu. Rev. Phytopathol. **53**:97–119.

Denoux, C., Galletti, R., Mammarella, N., Gopalan, S., Werck, D., De Lorenzo, G., Ferrari, S., Ausubel, F.M., and Dewdney, J. (2008). Activation of defense response pathways by OGs and Flg22 elicitors in *Arabidopsis* seedlings. Mol. Plant **1**:423–445.

Dobón, A., Canet, J.V., García-Andrade, J., Angulo, C., Neumetzler, L., Persson, S., and Vera, P. (2015). Novel disease susceptibility factors for fungal necrotrophic pathogens in *Arabidopsis*. PLoS Pathog. **11**:e1004800.

Dong, X. (2004). NPR1, all things considered. Curr. Opin. Plant Biol. **7**:547–552.

Dowen, R.H., Pelizzola, M., Schmitz, R.J., Lister, R., Dowen, J.M., Nery, J.R., Dixon, J.E., and Ecker, J.R. (2012). Widespread dynamic DNA methylation in response to biotic stress. Proc. Natl. Acad. Sci. U S A **109**:E2183–E2191.

Ferrer, J.L., Ravanel, S., Robert, M., and Dumas, R. (2004). Crystal structures of cobalamin-independent methionine synthase complexed with zinc, homocysteine, and methyltetrahydrofolate. J. Biol. Chem. **279**:44235–44238.

Gallardo, K., Job, C., Groot, S.P.C., Puype, M., Demol, H., Vandekerckhove, J., and Job, D. (2002). Importance of methionine biosynthesis for *Arabidopsis* seed germination and seedling growth. Physiol. Plant. **116**:238–247.

García-Andrade, J., Ramirez, V., Lopez, A., and Vera, P. (2013). Mediated plastid RNA editing in plant immunity. PLoS Pathog. **9**:e1003713.

Gerber, I.B., Laukens, K., De Vijlder, T., Witters, E., and Dubery, I.A. (2008). Proteomic profiling of cellular targets of lipopolysaccharide-induced signalling in Nicotiana tabacum BY-2 cells. Biochim. Biophys. Acta **1784**:1750–1762.

Giovanelli, J., Mudd, S.H., and Datko, A.H. (1985). Quantitative analysis of pathways of methionine metabolism and their regulation in lemna. Plant Physiol. **78**:555–560.

Groth, M., Moissiard, G., Wirtz, M., Wang, H., Garcia-Salinas, C., Ramos-Parra, P.A., Bischof, S., Feng, S., Cokus, S.J., John, A., et al. (2016). MTHFD1 controls DNA methylation in *Arabidopsis*. Nat. Commun. **7**:11640.

Hardham, A.R., Jones, D.A., and Takemoto, D. (2007). Cytoskeleton and cell wall function in penetration resistance. Curr. Opin. Plant Biol. **10**:342–348.

Ishikawa, T., Machida, C., Yoshioka, Y., Kitano, H., and Machida, Y. (2003). The GLOBULAR ARREST1 gene, which is involved in the biosynthesis of folates, is essential for embryogenesis in *Arabidopsis thaliana*. Plant J. **33**:235–244.

Jones, J.D., and Dangl, J.L. (2006). The plant immune system. Nature **444**:323–329.

Jordá, L., Coego, A., Conejero, V., and Vera, P. (1999). A genomic cluster containing four differentially regulated subtilisin-like processing protease genes is in tomato plants. J. Biol. Chem. **274**:2360–2365.

Kangasjarvi, S., Neukermans, J., Li, S., Aro, E.M., and Noctor, G. (2012). Photosynthesis, photorespiration, and light signalling in defence responses. J. Exp. Bot. **63**:1619–1636.

Loenen, W.A.M. (2006). Adenosylmethionine: jack of all trades and master of everything? Biochem. Soc. Trans. **34**:330–333.

Loizeau, K., De Brouwer, V., Gambonnet, B., Yu, A., Renou, J.P., Van Der Straeten, D., Lambert, W.E., Rebeille, F., and Ravanel, S. (2008).

A genome-wide and metabolic analysis determined the adaptive response of *Arabidopsis* cells to folate depletion induced by methotrexate. Plant Physiol. **148**:2083–2095.

Loizeau, K., Gambonnet, B., Zhang, G.F., Curien, G., Jabrin, S., Van Der Straeten, D., Lambert, W.E., Rebeille, F., and Ravanel, S. (2007). Regulation of one-carbon metabolism in *Arabidopsis*: the N-terminal regulatory domain of cystathionine gamma-synthase is cleaved in response to folate starvation. Plant Physiol. **145**:491–503.

López, A., Ramírez, V., García-Andrade, J., Flors, V., and Vera, P. (2011). The RNA silencing enzyme RNA polymerase v is required for plant immunity. PLoS Genet. **7**:e1002434.

Luna, E., Bruce, T.J., Roberts, M.R., Flors, V., and Ton, J. (2012). Next-generation systemic acquired resistance. Plant Physiol. **158**:844–853.

Luna, E., Pastor, V., Robert, J., Flors, V., Mauch-Mani, B., and Ton, J. (2011). Callose deposition: a multifaceted plant defense response. Mol. Plant Microbe Interact. **24**:183–193.

Martínez-Medina, A., Flors, V., Heil, M., Mauch-Mani, B., Pieterse, C.M., Pozo, M.J., Ton, J., van Dam, N.M., and Conrath, U. (2016). Recognizing plant defense priming. Trends Plant Sci. **21**:818–822.

Mauch-Mani, B., Baccelli, I., Luna, E., and Flors, V. (2017). Defense priming: an adaptive part of induced resistance. Annu. Rev. Plant Biol. **68**:485–512.

McCullough, J.L., and Maren, T.H. (1973). Inhibition of dihydropteroate synthetase from *Escherichia coli* by sulfones and sulfonamides. Antimicrob. Agents Chemother. **3**:665–669.

Navarova, H., Bernsdorff, F., Doring, A.C., and Zeier, J. (2012). Pipecolic acid, an endogenous mediator of defense amplification and priming, is a critical regulator of inducible plant immunity. Plant Cell **24**:5123–5141.

Noutoshi, Y., Ikeda, M., Saito, T., Osada, H., and Shirasu, K. (2012). Sulfonamides identified as plant immune-priming compounds in high-throughput chemical screening increase disease resistance in *Arabidopsis thaliana*. Front. Plant Sci. **3**:245.

Pato, M.L., and Brown, G.M. (1963). Mechanisms of resistance of Escherichia coli to sulfonamides. Arch. Biochem. Biophys. **103**:443–448.

Pavet, V., Quintero, C., Cecchini, N.M., Rosa, A.L., and Alvarez, M.E. (2006). *Arabidopsis* Displays centromeric DNA hypomethylation and cytological alterations of heterochromatin upon attack by *Pseudomonas syringae*. Mol. Plant Microbe Interact. **19**:577–587.

Pieterse, C.M., Van der Does, D., Zamioudis, C., Leon-Reyes, A., and Van Wees, S.C. (2012). Hormonal modulation of plant immunity. Annu. Rev. Cell Dev. Biol. **28**:489–521.

Prabhu, V., Lui, H., and King, J. (1997). *Arabidopsis* dihydropteroate synthase: general properties and inhibition by reaction product and sulfonamides. Phytochemistry **45**:23–27.

Ramirez, V., Gonzalez, B., Lopez, A., Castello, M.J., Gil, M.J., Zheng, B., Chen, P., and Vera, P.V. (2018). A 2-O-methyltransferase responsible for tRNA Anticodon modification is pivotal for resistance to *Pseudomonas syringae* DC3000 in *Arabidopsis*. Mol. Plant Microbe Interact. **31**:1323–1336.

Ramírez, V., López, A., Mauch-Mani, B., Gil, M.J., and Vera, P. (2013). An extracellular subtilase switch for immune priming in *Arabidopsis*. PLoS Pathog. **9**:e1003445.

Ravanel, S., Block, M.A., Rippert, P., Jabrin, S., Curien, G., Rebeille, F., and Douce, R. (2004). Methionine metabolism in plants: chloroplasts are autonomous for de novo methionine synthesis and can import S-adenosylmethionine from the cytosol. J. Biol. Chem. **279**:22548–22557.

Ravanel, S., Gakiere, B., Job, D., and Douce, R. (1998). The specific features of methionine biosynthesis and metabolism in plants. Proc. Natl. Acad. Sci. U S A **95**:7805–7812.

Rocha, P.S., Sheikh, M., Melchiorre, R., Fagard, M., Boutet, S., Loach, R., Moffatt, B., Wagner, C., Vaucheret, H., and Furner, I. (2005). The *Arabidopsis* HOMOLOGY-DEPENDENT GENE SILENCING1 gene codes for an S-adenosyl-L-homocysteine hydrolase required for DNA methylation-dependent gene silencing. Plant Cell **17**:404–417.

Roje, S. (2006). S-Adenosyl-L-methionine: beyond the universal methyl group donor. Phytochemistry **67**:1686–1698.

Schreiber, K., Ckurshumova, W., Peek, J., and Desveaux, D. (2008). A high-throughput chemical screen for resistance to *Pseudomonas syringae* in *Arabidopsis*. Plant J. **54**:522–531.

Shen, Y., Issakidis-Bourguet, E., and Zhou, D.X. (2016). Perspectives on the interactions between metabolism, redox, and epigenetics in plants. J. Exp. Bot. **67**:5291–5300.

Slaughter, A., Daniel, X., Flors, V., Luna, E., Hohn, B., and Mauch-Mani, B. (2012). Descendants of primed *Arabidopsis* plants exhibit resistance to biotic stress. Plant Physiol. **158**:835–843.

Storozhenko, S., Navarrete, O., Ravanel, S., De Brouwer, V., Chaerle, P., Zhang, G.F., Bastien, O., Lambert, W., Rebeille, F., and Van Der Straeten, D. (2007). Cytosolic hydroxymethyldihydropterin pyrophosphokinase/dihydropteroate synthase from *Arabidopsis thaliana*: a specific role in early development and stress response. J. Biol. Chem. **282**:10749–10761.

Torres, M.A. (2010). ROS in biotic interactions. Physiol. Plant **138**:414–429.

Toth, R., and van der Hoorn, R.A. (2010). Emerging principles in plant chemical genetics. Trends Plant Sci. **15**:81–88.

Urich, M.A., Nery, J.R., Lister, R., Schmitz, R.J., and Ecker, J.R. (2015). MethylC-seq library preparation for base-resolution whole-genome bisulfite sequencing. Nat. Protoc. **10**:475–483.

van Loon, L.C., Rep, M., and Pieterse, C.M. (2006). Significance of inducible defense-related proteins in infected plants. Annu. Rev. Phytopathol. **44**:135–162.

Vlot, A.C., Dempsey, D.A., and Klessig, D.F. (2009). Salicylic acid, a multifaceted hormone to combat disease. Annu. Rev. Phytopathol. **47**:177–206.

Wildermuth, M.C., Dewdney, J., Wu, G., and Ausubel, F.M. (2001). Isochorismate synthase is required to synthesize salicylic acid for plant defence. Nature **414**:562–565.

Yu, A., Lepere, G., Jay, F., Wang, J., Bapaume, L., Wang, Y., Abraham, A.L., Penterman, J., Fischer, R.L., Voinnet, O., et al. (2013). Dynamics and biological relevance of DNA demethylation in *Arabidopsis* antibacterial defense. Proc. Natl. Acad. Sci. U S A **110**:2389–2394.

Zeier, J. (2013). New insights into the regulation of plant immunity by amino acid metabolic pathways. Plant Cell Environ. **36**:2085–2103.

Zhang, H., Deng, X., Miki, D., Cutler, S., La, H., Hou, Y.J., Oh, J., and Zhu, J.K. (2012). Sulfamethazine suppresses epigenetic silencing in *Arabidopsis* by impairing folate synthesis. Plant Cell **24**:1230–1241.

Zhang, X., Yazaki, J., Sundaresan, A., Cokus, S., Chan, S.W.L., Chen, H., Henderson, I.R., Shinn, P., Pellegrini, M., Jacobsen, S.E., et al. (2006). Genome-wide high-resolution mapping and functional analysis of DNA methylation in *Arabidopsis*. Cell **126**:1189–1201.

Zhou, H.-R., Zhang, F.-F., Ma, Z.-Y., Huang, H.-W., Jiang, L., Cai, T., Zhu, J.-K., Zhang, C., and He, X.-J. (2013). Folate polyglutamylation is involved in chromatin silencing by maintaining global DNA methylation and histone H3K9 dimethylation in *Arabidopsis*. Plant Cell **25**:2545–2559.